

A theoretical study of the air-sea drag-saturation in very strong winds

Michael Stiassnie*¹ and David Andrade^{†2}

¹Department of Civil and Environmental Engineering, Technion,
Haifa, Israel

²Centre for Mathematical Sciences, University of Plymouth,
Plymouth PL4 8AA, UK

December 12, 2022

Abstract

The goal of this note is to provide a theoretical explanation for the saturation of the drag coefficient in strong wind conditions. The hydrodynamic model under consideration takes into account the important effects of airborne droplets of water in a thin layer above the water surface that effectively behave as a different fluid between the water and the air. Above this layer the model is coupled with a log-wind profile for the strong winds blowing above the sea. The main underlying mechanism governing the behavior of the drag coefficient is the Kelvin Helmholtz instability for capillary waves on the water surface and the continuity of shear stress along the intermediate interface.

1 Introduction

The shear-stress between air and sea is an important part of the momentum balance in the development of tropical cyclones.

*Email: miky@technion.ac.il

[†]Email: deandradep@gmail.com

In moderately wind conditions, with wind speeds less than 20 ms^{-1} , it is generally accepted that the drag coefficient increases with wind speed. However, for hurricane wind speeds (larger than 30 ms^{-1}), the experiments of Donelan et al. [2004] have convinced the meteorological community that the drag coefficient approaches a limiting value. A property which was basically accepted by the many hundreds of papers citing the above mentioned article.

A few of these papers try to provide some limited theoretical explanation to this phenomenon though it is widely accepted that the influence of water droplets near the water surface is one key factor responsible for the drag reduction. Following Soloviev and Lukas [2010], droplets are generated by the disruption of the air-sea interface due to wave breaking under strong winds. At wind speeds above 25 ms^{-1} , and these droplets effectively form a two-phase layer that covers the sea surface almost completely. A schematic representation is given in figure 1. Moreover an empirical parametrization of a similar layer, based on the surface wave spectrum, has been proposed by Iida et al. [1992].

In the current article, we provide a hydrodynamical explanation based on a linearized formulation for the air-sea system, including effects of airborne water droplets being carried by strong winds above the water surface. Our model hypothesis is that the droplets effectively create a different fluid between the water and the air characterized by having a different density $\rho_a < \rho < \rho_w$ (ρ_a is the density of the air and ρ_w is the density of the water), that moves with a constant horizontal velocity U_0 and has a height z_0 . This three parameters ρ , U_0 and z_0 are independent and are meant to model different environmental conditions. When the velocity U_0 is above a critical threshold, small capillary waves will appear as a result of the Kelvin-Helmholtz instability. Thus, we shall refer to this two-phase layer as the Kelvin-Helmholtz Layer (K.H. Layer).

This approach is different from the one proposed by Soloviev and Lukas [2010], where the influence of the droplets is accounted for by considering a stratified flow with linear velocity and density profiles within a thin strip between the water and the air. A different analytical model, which neglects the influence of the droplets altogether but also explains the drag saturation was proposed by Troitskaya and Rybushkina [2008].

Our model contains three different vertical length scales. A small scale for the height of the small capillary waves along the water surface, typically of the order of few millimeters, a small but somewhat larger scale for the thickness of the two-phase layer, typically less than two centimeters, and a much larger scale for the wind profile above the water. As for horizontal length scales we shall be dealing with short capillary waves with typical wavelengths of less than two centimeters,

that ride on the much longer waves generated by the storm.

In order to include the wind profile above the water surface we match a log wind profile with the K.H. Layer by requiring continuity of the horizontal velocity and stress between the K.H. Layer and the air. Then, based on the shear-stress, we compute the drag coefficient C_D for different values of U_{10} , the wind velocity at a height of $z = 10$ m.

Our model captures the saturation of the drag coefficient for strong winds and offers an explanation as to why it happens; it turns out that C_D strongly depends on the most unstable capillary wave that arises due to the K.H. instability, and reaches breaking conditions.

This paper is organized as follows. Section 2 deals with the basic hydrodynamics of the water and the K.H. Layer. In section 3 we introduce the appropriate wind profile and show how it is coupled with the hydrodynamic model. Section 4 discusses the drag coefficient and its saturation. Concluding remarks are provided in section 5.

2 Two Fluid Model

In this section we refer to the two lower domains in figure 1, namely the water and the K.H. Layer.

Our starting point are the linearized flow equations, (similar to those of Stiassnie et al. [2007]), for a system of two fluids separated by an interface.

Let (u_w, v_w) be the velocity field of the water, ρ_w its density and p_w the

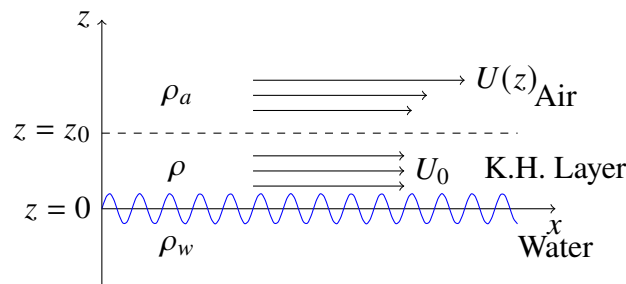


Figure 1: Schematic representation of the three flow domains.

pressure. The equations of motion for the water are

$$\frac{\partial u_w}{\partial x} + \frac{\partial v_w}{\partial z} = 0, \quad \text{in } z < 0. \quad (1)$$

$$\frac{\partial u_w}{\partial t} = -\frac{1}{\rho_w} \frac{\partial p_w}{\partial x}, \quad \text{in } z < 0. \quad (2)$$

$$\frac{\partial v_w}{\partial t} = -\frac{1}{\rho_w} \frac{\partial p_w}{\partial z}, \quad \text{in } z < 0. \quad (3)$$

Above the water surface, the K.H. Layer is represented by a fluid with constant density $\rho_w < \rho < \rho_a$, moving at constant speed U_0 and with height z_0 . We denote by (u, v) the wavy part of its velocity field and by p its pressure. The equations of motion are

$$\frac{\partial u}{\partial x} + \frac{\partial v}{\partial z} = 0, \quad \text{in } 0 < z < z_0. \quad (4)$$

$$\frac{\partial u}{\partial t} + U_0 \frac{\partial u}{\partial x} = -\frac{1}{\rho} \frac{\partial p}{\partial x}, \quad \text{in } 0 < z < z_0. \quad (5)$$

$$\frac{\partial v}{\partial t} + U_0 \frac{\partial v}{\partial x} = -\frac{1}{\rho} \frac{\partial p}{\partial z}, \quad \text{in } 0 < z < z_0. \quad (6)$$

Along the mean interface, $z = 0$, we have the kinematic boundary conditions:

$$v_w = \frac{\partial \eta}{\partial t}, \quad \text{on } z = 0, \quad (7)$$

$$v = \frac{\partial \eta}{\partial t} + U_0 \frac{\partial \eta}{\partial x}, \quad \text{on } z = 0, \quad (8)$$

where $z = \eta(x, t)$ is the interface elevation. Additionally the Bernoulli equation is given by

$$p_w - g\rho_w\eta = p - g\rho\eta - \rho_w\tau \frac{\partial^2 \eta}{\partial x^2}. \quad (9)$$

Here we take $g = 9.81 \text{ms}^{-2}$ for the acceleration due to gravity and $\tau = 7.4 \times 10^{-5} \text{m}^3\text{s}^{-2}$ for the ratio between surface tension and the density of the water, which is $\rho_w = 1000 \text{Kgm}^{-3}$. The density of the air is $\rho_a = 1.2 \text{Kgm}^{-3}$.

We look for wave-like solutions determined by a wave number $k > 0$ and, in anticipation of instability, a complex frequency ω . The linearized interface is denoted by

$$\eta = \text{Re} \left[a_0 e^{i(kx - \omega t)} \right], \quad (10)$$

where a_0 is the initial wave amplitude.

We assume that the height of the layer z_0 is comparable to the typical wave length of η , i.e. $\exp(-kz_0)$ is small, thus allowing us to replace the domain of equations (4) from $0 < z < z_0$ by $0 < z$.

In general, one can introduce a velocity potential for each fluid from which one can retrieve the velocity fields and the pressures. The potentials are

$$\phi_w = \frac{a_0}{k} e^{kz} \operatorname{Im} \left[\omega e^{i(kx - \omega t)} \right], \quad (11)$$

$$\phi = -\frac{a_0}{k} e^{-kz} \operatorname{Im} \left[\omega e^{i(kx - \omega t)} \right] + a_0 U_0 e^{-kz} \operatorname{Im} \left[e^{i(kx - \omega t)} \right]. \quad (12)$$

The pressure of the water is found to be

$$p_w = \rho_w \frac{a_0}{k} e^{kz} \operatorname{Re} \left[\omega^2 e^{i(kx - \omega t)} \right], \quad (13)$$

and the pressure in the K.H. Layer is

$$p = -\rho \frac{a_0}{k} e^{-kz} \operatorname{Re} \left[(\omega - kU_0)^2 e^{i(kx - \omega t)} \right]. \quad (14)$$

Last, substituting equations (10), (13) and (14) in the Bernoulli equation (9) yields the following dispersion relation

$$\omega = \frac{\rho_d k U_0}{1 + \rho_d} \pm \left[\frac{gk(1 - \rho_d)}{1 + \rho_d} + \frac{\tau k^3}{1 + \rho_d} - \frac{\rho_d k^2 U_0^2}{(1 + \rho_d)^2} \right]^{1/2} = \frac{\rho_d k U_0}{1 + \rho_d} \pm P^{1/2}(k), \quad (15)$$

where $\rho_d = \rho/\rho_w$ is the relative density and $P(k)$ is a degree three polynomial, which always has $k = 0$ as a real root.

2.1 Kelvin Helmholtz Instability Considerations

Let U_{cr} be the critical speed, given by

$$U_{cr} = (1 + \rho_d - \rho_d^2 - \rho_d^3)^{1/4} \left[\frac{4g\tau}{\rho_d^2} \right]^{1/4}. \quad (16)$$

When $U_0 \leq U_{cr}$, $P(k) \geq 0$ and so ω is always real. On the other hand when $U_0 > U_{cr}$, P has two additional positive roots k_1 and k_2 . For $k_1 < k < k_2$,

$P(k) < 0$ which leads to a complex frequency ω , implying instabilities with growth rates given by $(-P(k))^{1/2}$.

The critical wave numbers are

$$k_1 = \frac{\rho_d U_0^2 - \sqrt{\rho_d^2 U_0^4 - 4g\tau(1 + \rho_d - \rho_d^2 - \rho_d^3)}}{2\tau(1 + \rho_d)}. \quad (17)$$

$$k_2 = \frac{\rho_d U_0^2 + \sqrt{\rho_d^2 U_0^4 - 4g\tau(1 + \rho_d - \rho_d^2 - \rho_d^3)}}{2\tau(1 + \rho_d)}. \quad (18)$$

The imaginary part of the frequency, i.e. the growth rate, is given by

$$\beta = \text{Im}[\omega] = \frac{1}{1 + \rho_d} \left(\rho_d U_0^2 k^2 - (1 - \rho_d^2) g k - (1 + \rho_d) \tau k^3 \right)^{1/2}, \quad (19)$$

whereas its real part is

$$\alpha = \text{Re}[\omega] = \frac{\rho_d k U_0}{1 + \rho_d}. \quad (20)$$

Note that in case of instability, all unstable waves with $k_1 < k < k_2$ propagate with the same phase velocity

$$c = \frac{\alpha}{k} = \frac{\rho_d U_0}{1 + \rho_d}, \quad (21)$$

which does not depend on k , while its amplitude grows exponentially according to

$$a = a_0 e^{\beta t}, \quad (22)$$

where a_0 is the initial amplitude of the wave, as given in (10).

The wave with maximum growth rate, for a given $U_0 > U_{cr}$, is

$$k_m = \frac{1}{1 + \rho_d} \left(\frac{\rho_d U_0^2}{3\tau} + \left[\left(\frac{\rho_d U_0^2}{3\tau} \right)^2 - (1 + \rho_d - \rho_d^2 - \rho_d^3) \frac{g}{3\tau} \right]^{1/2} \right). \quad (23)$$

2.2 Wave Induced Stress

Following Phillips [1966], equation 3.2.11, page 28, the mean momentum per unit area is given by

$$M = -\rho_w \overline{\left(\phi_w(x, 0, t) \frac{\partial \eta}{\partial x}(x, t) \right)}, \quad (24)$$

where the bar denotes averaging over one wavelength. This equation is correct to second order.

By substituting equations (10),(11) into equation (24) and averaging, it follows that

$$M = \rho_w \frac{1}{2} \alpha a^2. \quad (25)$$

Let σ be the air-sea shear-stress. This is obtained directly from

$$\sigma = \frac{dM}{dt} = \rho_w \alpha \beta a^2. \quad (26)$$

Note that in case of stability, (i.e. $\beta = 0$), M is constant and there is no shear stress induced by the wave on the water surface.

According to (22) any unstable wave can grow indefinitely with time. In reality, an unstable wave will grow exponentially until it reaches its maximum amplitude and breaks. Once the wave breaks it releases water particles that are carried by the wind and join the K.H. Layer. These droplets eventually fall down and coalesce into the water and their momentum is conveyed in the form of stress onto the water surface.

The maximum amplitude that a propagating wave can reach is obtained from

$$a = \frac{\chi(k)}{k}, \quad (27)$$

where χ denotes the maximum wave steepness. This value is estimated as

$$\chi(k) = 2.292 - \frac{3.630 \times 10^2}{k} - \frac{5.017 \times 10^5}{k^2} + \frac{2.565 \times 10^8}{k^3} - \frac{3.545 \times 10^{10}}{k^4}. \quad (28)$$

This equation was obtained through a polynomial fit of the results of Hogan [1980] (p. 434). There, the maximum wave steepness is denoted by h_{max} and it is given as a function of his dimensionless parameter κ . In equation (28), $\chi \equiv h_{max}$ and k denotes the wave number in m^{-1} .

Equation (28) recovers the results of Hogan for wave numbers $k = 325.65, 364.09, 814.14, 1151.37 \text{ m}^{-1}$, since these were the values used for the polynomial interpolation. Moreover, as k tends to infinity, χ recovers the asymptotic value for extremely short waves, given also in Hogan [1980]. In this article, all the computations involve waves with $k > 325 \text{ m}^{-1}$ (wave lengths smaller than 1.9 cm), therefore this interpolation is enough for our purposes.

3 Coupling the K.H. Layer to the wind profile

So far, our model describes the motion of the water surface under the influence of, mainly, the K.H. Layer above it. In this section we couple a logarithmic wind profile with the K.H. Layer to include the effects of the wind blowing above it.

The criteria to match the horizontal wind profile with the dynamics of the K.H. Layer is that of continuity in velocity and stress. The logarithmic profile that we chose for the wind is

$$U(z) = \frac{u_*}{\kappa} \ln\left(\frac{z}{z_0}\right) + U_0, \quad \text{for } z > z_0. \quad (29)$$

Note that this logarithmic wind profile is only defined above z_0 . In our coupling, the thickness of the K.H. Layer is taken equal to the wavelength of the most unstable wave k_m . Hence

$$z_0 = 2\pi/k_m. \quad (30)$$

In equation (29) $\kappa = 0.41$ is the von Kármán constant and u_* is the frictional velocity which is related to the shear-stress by

$$u_* = \left[\frac{\sigma}{\rho_a} \right]^{1/2}. \quad (31)$$

Once the wind profile is determined, the drag coefficient based on U_{10} , the wind velocity at $z = 10$ m, is given by

$$C_D = \frac{u_*^2}{U_{10}^2}. \quad (32)$$

4 Saturation of the Drag Coefficient

Equations (29) and (32) are used as parametric equations of the functional relation between the drag coefficient C_D and the wind velocity at 10 m height U_{10} , for a chosen ρ_d .

In figure 2 we plot the drag coefficient as a function of U_{10} , for different values of the parameter ρ_d . We use $\rho_d = 0.0012, 0.0024, 0.0048, 0.0096$ and 0.0192 . Note that $\rho_d = 0.0012$ assumes that there are no droplets in the K.H. Layer.

According to our model the typical behavior of C_D can be described as a bounded function of U_{10} . It grows monotonically once the velocity inside the

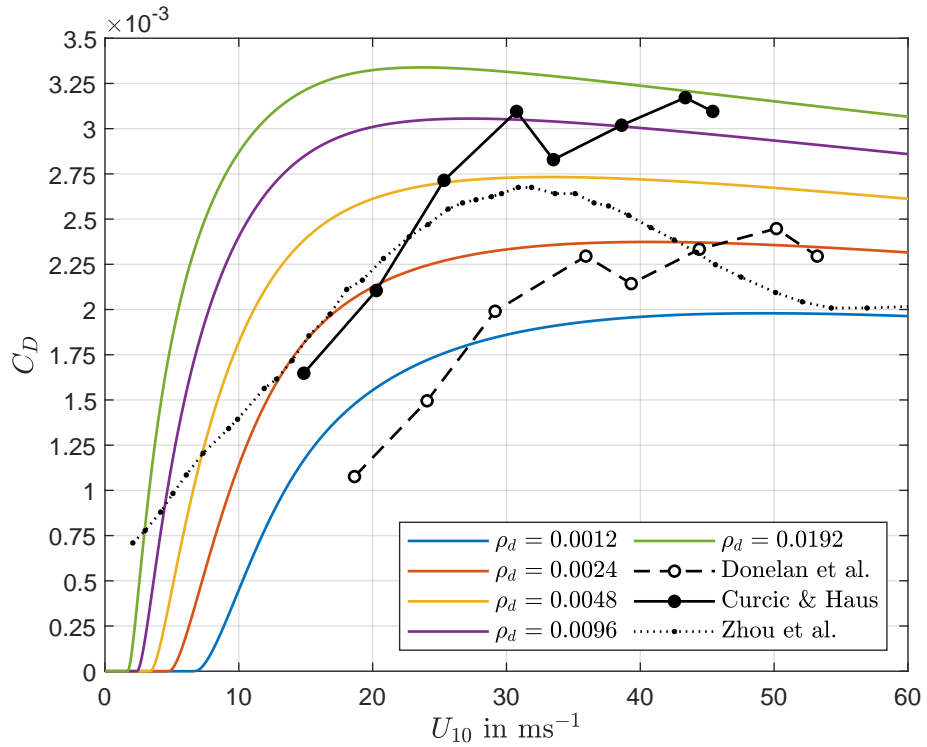


Figure 2: Drag coefficient as a function of U_{10} , for different values of ρ_d . The black broken line shows the original presentation of the measurements taken from Donelan et al. [2004]. The black solid line is the recently corrected presentation of the same measurements as reported in figure 3 of Curcic and Haus [2020]. The dotted line shows C_D as implemented in the Geophysical Fluid Dynamics Laboratory hurricane model, reported by Zhou et al. [2022].

K.H. Layer exceeds the critical speed U_{cr} , then it reaches a maximum followed by a slow decrease as the wind speed U_{10} increases. *Thus, our model captures the saturation of the drag coefficient in accordance with the experimental results of Donelan et al. [2004].*

The theoretical values of the drag coefficient drawn from our model are compared with the original experimental results reported in Donelan et al. [2004] and given by the broken line with empty dots in figure 2. However, due to an error in processing the experimental data, the corrected results of the same experiment of Donelan et al., were recently published by Curcic and Haus [2020] and are also given in figure 2 in the solid line with full dots. We also compare our model with the current implementation of C_D in the Geophysical Fluid Dynamics Laboratory hurricane model, recently reported by Zhou et al. [2022] and given by the dotted line in figure 2.

From figure 2, one can see that our model predicts a range of values for C_D which is in fairly good agreement with experimental measurements. Moreover, for very strong winds the hypothesis of the K.H. Layer seems valid and even the apparent discrepancy between different results is accounted for by choosing different values of ρ_d .

According to the results reported by Curcic and Haus [2020] for $U_{10} > 30$ ms^{-1} the effect of droplets account for an eight-fold increase of the air density near the water surface but, according to the values reported by Zhou et al. [2022], for $U_{10} > 50$ ms^{-1} the effect of droplets should be ignored.

Discrepancies between different experimental measurements of C_D , indicate that the spectral conditions in the vicinity of the measurement point can be different for the same wind speed U_{10} and our model suggests that such environmental conditions are critical for the determination of ρ_d and the exact drag.

Specific values of all the parameters of the model, for a given U_{10} and a given ρ_d , can be obtained by solving numerically the following equation for U_0

$$U_{10} = \frac{u_*(\rho_d, U_0)}{\kappa} \ln \left(\frac{10}{z_0(\rho_d, U_0)} \right) + U_0. \quad (33)$$

Resulting values of C_D , as well as other parameters of the wind and the wave, for $U_{10} = 20, 30, 40, 50, 60$ ms^{-1} are tabulated in appendix 5 in tables 2 - 6.

At first glance, the wind model given by equation (29) resembles the following logarithmic wind profile which is often used in wave forecasting models:

$$U_\alpha(z) = \frac{u_*}{\kappa} \ln \left(1 + \frac{z}{z_\alpha} \right), \quad (34)$$

		U_{10}						
		20	30	40	50	60	80	100
ρ_d	0.0012	1.55	1.86	1.96	1.98	1.96	1.89	1.81
	0.0024	2.12	2.23	2.37	2.35	2.31	2.21	2.10
	0.0048	2.61	2.73	2.72	2.67	2.61	2.48	2.36
	0.0096	3.01	3.05	3.00	2.93	2.86	2.72	2.57
	0.0192	3.32	3.31	3.24	3.15	3.07	2.90	2.76

Table 1: Values of $C_D \times 10^3$ as a function of U_{10} in ms^{-1} and ρ_d . The largest value in each row is in bold.

see equations (2.31) and (2.32) in Komen et al. [1996] page 83, with z_α given by Charnok's relation with constant close to $\tilde{\alpha} = 0.0144$

$$z_\alpha = \tilde{\alpha} \frac{u_*^2}{g}. \quad (35)$$

However this model *does not* capture the saturation of the drag coefficient. Instead, it predicts that C_D grows monotonically as U_{10} increases.

5 Concluding remarks

In the present article we studied the saturation of the drag coefficient at high wind speeds based on the Kelvin Helmholtz instability. This study follows some previous authors and uses the term “drag saturation” in its title. However Table 1, in which we have highlighted the largest values of C_D in each line, as well as figure 2, indicate that the term “drag maximizing” would probably be more adequate.

Our model has one basic assumption which is the very existence of the K.H. Layer. This layer is made of an air and droplets mixture. It is characterized by three constants: (i) A thickness z_0 . (ii) a uniform density ρ_d . (iii) A uniform velocity U_0 . All three parameters relate in a way to the prevailing environmental conditions.

Given the narrowness, of less than two centimeters, of the K.H. Layer and its rather complex surroundings, its physical existence might be difficult to detect, but its phenomenological value has been demonstrated herein. Moreover, equation (29) enables us to find the frictional velocity u_* from any two measured values of

a wind profile, say U_{10} and $U_h = U(z = h)$, given by

$$\frac{u_*}{\kappa} = \frac{U_{10} - U_h}{\ln(10/h)}. \quad (36)$$

Once we know u_* we can calculate C_D from equation (32) and obtain ρ_d by interpolating the values in Table 1. Having U_{10} and ρ_d one can get U_0 , as well as other interesting values, by interpolating in tables 2 - 6.

It is quite clear that, under strong winds, a certain part of the gravity waves break, releasing a lot of droplets into the air. These droplets fall until they reach the K.H. Layer and contribute to the increase in its ρ_d . The increase of ρ_d in its turn, as well as the mechanism of the K.H. Layer, are both responsible for the increase in C_D . Specifically, the resistance that the gravity wave spectrum applies on the wind is represented by the fact that ρ_d in the K.H. Layer is larger than $\rho_d = 0.0012$, and in the examples herein reaches values up to 0.0192. This phenomenon is demonstrated in tables 2 - 6 which are given in the appendix 5. For $U_{10} = 20 \text{ ms}^{-1}$ one can see that the presence of a gravity wave spectrum increases C_D from 1.55×10^{-3} to 3.22×10^{-3} whereas for $U_{10} = 50 \text{ ms}^{-1}$ the increase is from 1.98×10^{-3} to 3.15×10^{-3} .

Unfortunately all laboratory measured droplet mass concentrations, see Veron et al. [2012], Mehta et al. [2019], seem to be given for z values larger than those relevant for the K.H. Layer mentioned herein.

Last, we have tried to include viscous effects into the two fluid model given in section 2. In fact we adapted the ideas of the paper by Dias et al. [2008] to our two fluid model, resulting in the following new dispersion relation:

$$\omega = \frac{\rho_d k U_0}{1 + \rho_d} \pm \left[\frac{gk(1 - \rho_d)}{1 + \rho_d} + \frac{\tau k^3}{1 + \rho_d} - \frac{\rho_d k^2 U_0^2}{(1 + \rho_d)^2} - \frac{4\tilde{\nu}^2 k^4}{1 + \rho_d} \right]^{1/2}, \quad (37)$$

which turns out almost identical to equation (15) except for the additional last term under the square root. This term is proportional to $\tilde{\nu}^2$ with $\tilde{\nu} = 10^{-6} \text{ m}^2 \text{ s}^{-1}$ being the kinematic viscosity of the water. However the plots of C_D were virtually unaffected by the inclusion of viscosity hence we opted for the inviscid model for our computations.

A Values of C_D and other parameters for $U_{10} = 20,30,40,50$ and 60 ms^{-1} and $\rho_d = 0.0012,0.0024, 0.0048, 0.0096$ and 0.0192

ρ_d	0.00120000	0.00240000	0.00480000	0.00960000	0.01920000
U_0	7.25391253	5.11707499	3.58116224	2.50004897	1.74800569
k_1	204.36711960	206.37666684	215.39683288	228.47513433	243.18429757
k_2	647.89525217	640.81568634	612.50317137	574.65736613	534.66556670
k_m	475.31904776	471.24973521	455.35596769	434.75608901	413.83770156
c_m	0.00869426	0.01225158	0.01710746	0.02377226	0.03292946
a_m	2.11019263	2.11359792	2.12742418	2.14687603	2.16869999
χ_m	1.00301475	0.99603246	0.96873530	0.93336742	0.89748982
z_0	1.32188797	1.33330267	1.37984033	1.44522077	1.51827281
α_m	4.13254830	5.77355204	7.78998534	10.33513322	13.62745354
β_m	40.53074887	39.52838919	35.56096481	30.32525290	24.89099215
σ_m	0.74584188	1.01952281	1.25377140	1.44455620	1.59534961
u_*	0.78837485	0.92173876	1.02215923	1.09717676	1.15302125
C_D	0.00155384	0.00212401	0.00261202	0.00300949	0.00332365

Table 2: Resulting parameters of the waves and the wind profile obtained for the wind velocity $U_{10} = 20 \text{ ms}^{-1}$. All units are in m.k.s., except for a_m and z_0 which are in mm and cm respectively.

ρ_d	0.00120000	0.00240000	0.00480000	0.00960000	0.01920000
U_0	8.12240589	5.65168609	3.90409150	2.69179163	1.85970528
k_1	143.06863503	149.63220356	160.15123753	173.26035481	187.69111875
k_2	925.48926928	883.82983249	823.79159398	757.78973823	692.74599212
k_m	643.81816677	617.59610751	580.16028169	539.59262910	500.33451398
c_m	0.00973520	0.01353157	0.01865012	0.02559548	0.03503369
a_m	1.97808203	1.99972788	2.02938685	2.06027852	2.09014391
χ_m	1.27352515	1.23502415	1.17736965	1.11171110	1.04577114
z_0	0.97592544	1.01736155	1.08300852	1.16443127	1.25579690
α_m	6.26770172	8.35704548	10.82005807	13.81113397	17.52856644
β_m	81.92538212	75.36770969	66.12199017	56.22588247	46.74729661
σ_m	2.00916401	2.51871996	2.94649151	3.29622984	3.57977126
u_*	1.29394874	1.44876958	1.56697466	1.65736484	1.72717767
C_D	0.00186034	0.00233215	0.00272823	0.00305206	0.00331460

Table 3: Resulting parameters of the waves and the wind profile obtained for the wind velocity $U_{10} = 30 \text{ ms}^{-1}$. All units are in m.k.s., except for a_m and z_0 which are in mm and cm respectively.

ρ_d	0.00120000	0.00240000	0.00480000	0.00960000	0.01920000
U_0	9.00682050	6.19590298	4.23468236	2.89154818	1.98037392
k_1	109.97839236	117.61111590	128.15306989	140.60988847	153.97783839
k_2	1203.95000912	1124.46348623	1029.48172332	933.75309762	844.42197415
k_m	822.27670843	770.86300389	709.79947992	648.78519052	592.44400475
c_m	0.01079523	0.01483456	0.02022937	0.02749491	0.03730689
a_m	1.81578776	1.86432821	1.92054710	1.97389899	2.01980612
χ_m	1.49307998	1.43714165	1.36320333	1.28063643	1.19662203
z_0	0.76412055	0.81508456	0.88520568	0.96845387	1.06055345
α_m	8.87666645	11.43541672	14.35879938	17.83829132	22.10224156
β_m	128.54088418	114.65175146	98.58995495	82.98439006	68.93807249
σ_m	3.76202218	4.55698326	5.22156537	5.76765809	6.21605468
u_*	1.77059834	1.94871395	2.08597806	2.19234617	2.27597135
C_D	0.00195939	0.00237343	0.00271957	0.00300399	0.00323753

Table 4: Resulting parameters of the waves and the wind profile obtained for the wind velocity $U_{10} = 40 \text{ ms}^{-1}$. All units are in m.k.s., except for a_m and z_0 which are in mm and cm respectively.

ρ_d	0.00120000	0.00240000	0.00480000	0.00960000	0.01920000
U_0	9.91064965	6.74962643	4.56925792	3.09284650	2.10192329
k_1	88.11061541	95.96978041	106.26580733	118.17980799	130.82055086
k_2	1502.75294149	1378.03175996	1241.52111165	1110.97590321	993.89789611
k_m	1017.18521740	935.54754971	846.57772108	762.00302075	686.69752763
c_m	0.01187853	0.01616032	0.02182767	0.02940900	0.03959667
a_m	1.63344375	1.70856885	1.79269450	1.87260901	1.94114848
χ_m	1.66151483	1.59844740	1.51765522	1.42693372	1.33298186
z_0	0.61770317	0.67160513	0.74218647	0.82456173	0.91498586
α_m	12.08266040	15.11874653	18.47881506	22.40974683	27.19093612
β_m	184.16439007	160.17975236	135.01569572	112.02080550	92.27182360
σ_m	5.93713047	7.06949468	8.01809042	8.80298293	9.45389506
u_*	2.22432208	2.42718882	2.58490658	2.70847173	2.80682131
C_D	0.00197904	0.00235650	0.00267270	0.00293433	0.00315130

Table 5: Resulting parameters of the waves and the wind profile obtained for the wind velocity $U_{10} = 50 \text{ ms}^{-1}$. All units are in m.k.s., except for a_m and z_0 which are in mm and cm respectively.

ρ_d	0.00120000	0.00240000	0.00480000	0.00960000	0.01920000
U_0	10.83792400	7.31610636	4.90998876	3.29668184	2.22429052
k_1	72.34905063	80.06691079	89.97458947	101.37545661	113.45441710
k_2	1830.13440172	1651.73608059	1466.31670134	1295.13516690	1146.03092231
k_m	1232.51238793	1114.99884247	993.25165739	881.35035656	784.40377162
c_m	0.01298992	0.01751662	0.02345536	0.03134721	0.04190186
a_m	1.45190316	1.54766639	1.65517824	1.75966319	1.85161407
χ_m	1.78948863	1.72564624	1.64400853	1.55087978	1.45241306
z_0	0.50978679	0.56351496	0.63258745	0.71290438	0.80101416
α_m	16.01023842	19.53100589	23.29707551	27.62787687	32.86797880
β_m	251.31820418	213.83032503	176.79770258	144.39197833	117.55236566
σ_m	8.48197617	10.00342250	11.28411651	12.35235254	13.24662721
u_*	2.65863000	2.88724530	3.06650133	3.20836829	3.32247739
C_D	0.00196342	0.00231561	0.00261206	0.00285934	0.00306635

Table 6: Resulting parameters of the waves and the wind profile obtained for the wind velocity $U_{10} = 60 \text{ ms}^{-1}$. All units are in m.k.s., except for a_m and z_0 which are in mm and cm respectively.

References

- M. Curcic and B. K. Haus. Revised estimates of ocean surface drag in strong winds. *Geophysical Research Letters*, 47(10):e2020GL087647, 2020.
- F. Dias, A. I. Dyachenko, and V. E. Zakharov. Theory of weakly damped free-surface flows: A new formulation based on potential flow solutions. *Physics Letters A*, 372(8):1297–1302, 2008. ISSN 0375-9601. doi: <https://doi.org/10.1016/j.physleta.2007.09.027>. URL <https://www.sciencedirect.com/science/article/pii/S037596010701345X>.
- M. A. Donelan, B. K. Haus, N. Reul, W.J. Plant, M. Stiassnie, H.C. Graber, O.B. Brown, and E.S. Saltzman. On the limiting aerodynamic roughness of the ocean in very strong winds. *Geophysical Research Letters*, 31(18), 2004.
- S.J. Hogan. Some effects of surface tension on steep water waves. part 2. *Journal of Fluid Mechanics*, 96(3):417–445, 1980.
- N. Iida, Y. Toba, and M. Chaen. A new expression for the production rate of sea water droplets on the sea surface. *Journal of Oceanography*, 48(4):439–460, 1992.
- G. J. Komen, L. Cavaleri, M. Donelan, K. Hasselmann, S. Hasselmann, and P.A.E.M. Janssen. *Dynamics and modelling of ocean waves*. Cambridge University Press, 1996.
- S. Mehta, D. G. Ortiz-Suslow, A. W. Smith, and B. K. Haus. A laboratory investigation of spume generation in high winds for fresh and seawater. *Journal of Geophysical Research: Atmospheres*, 124(21):11297–11312, 2019.
- O. M. Phillips. *The Dynamics of the Upper Ocean*. Cambridge University Press, 1966. ISBN 9780521214216.
- A. Soloviev and R. Lukas. Effects of bubbles and sea spray on air–sea exchange in hurricane conditions. *Boundary-layer meteorology*, 136(3):365–376, 2010.
- M Stiassnie, Y Agnon, and PAEM Janssen. Temporal and spatial growth of wind waves. *Journal of physical oceanography*, 37(1):106–114, 2007.
- Yu. I Troitskaya and G. V. Rybushkina. Quasi-linear model of interaction of surface waves with strong and hurricane winds. *Izvestiya, Atmospheric and*

Oceanic Physics, 44:621 – 645, 2008. doi: 10.1134/S0001433808050083.
URL <https://doi.org/10.1134/S0001433808050083>.

F. Veron, C. Hopkins, E.L. Harrison, and J.A. Mueller. Sea spray spume droplet production in high wind speeds. *Geophysical Research Letters*, 39(16), 2012.

X. Zhou, T. Hara, I. Ginis, E. D’Asaro, J. Hsu, and B.G. Reichl. Drag coefficient and its sea state dependence under tropical cyclones. *Journal of Physical Oceanography*, 52(7):1447 – 1470, 2022. doi: 10.1175/JPO-D-21-0246.1. URL <https://journals.ametsoc.org/view/journals/phoc/52/7/JPO-D-21-0246.1.xml>.